RESEARCH ACTIVITIES

Photo-Molecular Science

We study the interaction between molecules and optical fields with its possible applications to active control of molecular functionality and reactivity. We also develop novel light sources to promote those studies. Two research facilities, the Laser Research Center for Molecular Science and the UVSOR, closely collaborate with the Department.

The core topics of the Department include ultrahigh-precision coherent control of gas- and condensed-phase molecules, high-resolution optical microscopy applied to nanomaterials, synchrotron-based spectroscopy of core-excited molecules and solid-state materials, vacuum-UV photochemistry, and the development of novel laser- and synchrotron-radiation sources.

Development of Advanced Near-Field Spectroscopy/Imaging and Application to Nanomaterials

Department of Photo-Molecular Science
Division of Photo-Molecular Science I

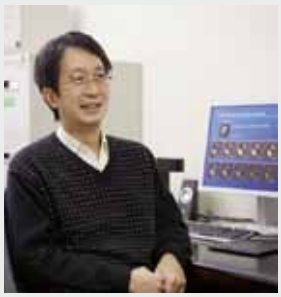

OKAMOTO, Hiromi
Professor

NARUSHIMA, Tetsuya
Assistant Professor

NISHIYAMA, Yoshio
IMS Research Assistant Professor

KOWAKA, Yasuyuki	Post-Doctoral Fellow	ISHIKAWA, Akiko	Technical Fellow
HASHIYADA, Shun	Graduate Student	NOMURA, Emiko	Secretary
WU, Huijun	Technical Fellow	YAMASAKI, Yumi	Secretary

There is much demand for the study of local optical properties of molecular assemblies and materials, to understand nanoscale physical and chemical phenomena and/or to construct nanoscale optoelectronic devices. Scanning near-field optical microscopy (SNOM) is an imaging method that enables spatial resolution beyond the diffraction limit of light. Combination of this technique with various advanced spectroscopic methods may provide direct probing methods for dynamics in nanomaterials and nanoscale functionalities. It may yield essential and basic knowledge to analyze origins of characteristic features of the nanomaterial systems. We have constructed apparatuses of near-field spectroscopy and microscopy for excited-state studies of nanomaterials, with the feasibilities of nonlinear and time-resolved measurements. The developed apparatuses enable near-field measurements of two-photon induced emission, femtosecond time-resolved signals, and circular dichroism, in addition to conventional transmission, emission, and Raman-scattering. Based on these methods, we are investigating the characteristic spatiotemporal behavior of various metal-nanostructure systems and molecular assemblies.

1. Visualization of Localized Optical Fields and Plasmon Wavefunctions in Metal Nanostructures

We reported that wavefunctions of localized plasmon resonances of chemically synthesized metal (Au and Ag) nanoparticles are visualized by near-field transmission or two-photon excitation measurements.[1,2] The same methods were also applied to Au nanoparticle assemblies to visualize confined optical fields.[1,2]

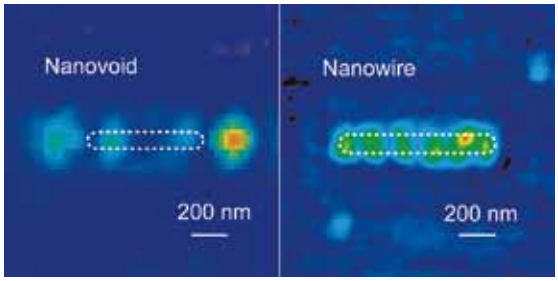

Figure 1. Near-field two-photon excitation images of an elongated rectangular nanoaperture on Au film (630 nm^l × 90 nm^w × 30 nm^t) observed at 810 nm (left) and a nanowire (860 nm^l × 100 nm^w × 30 nm^t) observed at 800 nm (right).

We have extended the studies to a variety of metal nanostructures including those manufactured by the electron-beam lithography technique, in part as collaboration with researchers of other institutions. For elongated rectangular apertures opened on thin Au film, we observed spatially oscillating features in the apertures that are arising from localized surface plasmon resonance of the nanostructures (Figure 1).[3] The elongated rectangular aperture corresponds to an inverted structure of a nanorod, and the oscillating structure observed may have a similar origin to that for nanorods.

For one-dimensional linear array of spherical Au nanoparticles, we revealed that enhanced fields (observed at ~800 nm) tend to localize near the ends of the arrays, when the number of particles exceeds 5 (Figure 2).[4] This observation is interpreted as a result of plasmon propagation among the particles and existence of localized modes near the boundaries

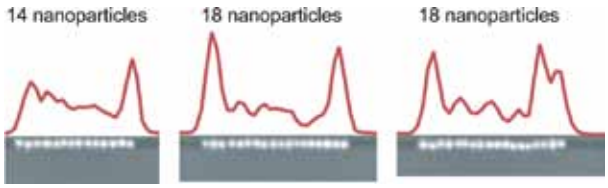

Figure 2. Plots of near-field two-photon excitation signals for the linear arrays of spherical Au nanoparticles (diameters ~100 nm) along the chain axis, observed at 785 nm. Images below the plot are corresponding scanning electron micrographs.

of the arrays.

We also tried to observe enhanced field characteristics for assemblies of particles with different shapes, specifically Ag nanowires joined with Ag nanospheres.[5] We have found that enhanced fields at the interstitial sites, polarized *perpendicular* to the long axis of the wire, are excited when the incident photons are polarized *along* the long axis of the wire. Such studies are essential as bases for designing unique optical properties and functions of metal nanostructures.

2. Near-Field Circular Dichroism Microscopy of Nanomaterials

Circular dichroism (CD) spectroscopy is widely used in the studies of chiral materials and magnetism. Some of nanomaterials composed of achiral molecules are reported to show CD activities arising from the nanoscale chirality. Two-dimensionally chiral metal nanostructures also show CD activities. Investigation of nanoscale local CD may provide valuable information on the origins of CD activities of such materials. For this purpose, we are developing an apparatus for near-field CD microscopy based on polarization modulation technique with a photoelastic modulator, and measuring CD images of nanoscale chiral materials.

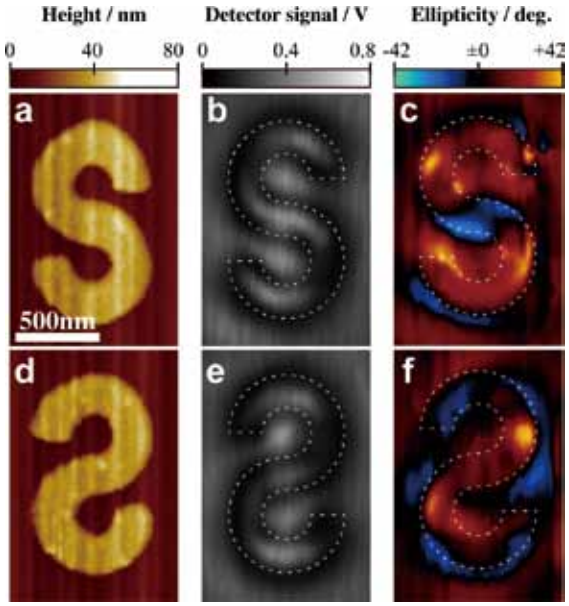

Figure 3. Topography (a, d), near-field transmission (b, e), and near-field CD (c, f) images of an S-shaped Au nanostructure (a, b, c) and its mirror-imaged structure (d, e, f) observed at 633 nm.

Here we report on a nanoscale CD imaging for a two-dimensional chiral pair of Au nanostructures to elucidate the relationship between nanoscale chirality and CD activity.[6] We adopted a two-dimensional "S"-shaped nanostructure (1200 nm × 700 nm, Au film thickness 40 nm) prepared with electron-beam lithography technique and its mirrored structure as the samples. The chiral pair exhibited very high local ellipticity at the center of the S-structure, and signals of both handedness coexisted in one nanostructure (Figure 3).

Based upon a model analysis for rotating dipole induced by the circular polarized light, we propose a mechanism of the strong CD signal at the center of the S-structure as mentioned in the following. If the rotational velocity of the induced polarization, in addition to the magnitude, changes reflecting the asymmetric structure of the sample, it produces perceivable difference between the optical response to the left-handed circular polarized light and that to the right-handed one, which yields a strong CD signal. This result indicates that it yields strong chiral field at the center of the structure, which may be potentially utilized for analysis of chiral molecules, chiral reaction fields, and so forth.

3. Construction of Apparatuses for Sub-20-fs Ultrafast Near-Field Spectroscopy

Surface plasmons of noble metal nanoparticles have very short lifetimes in the range of ~2-20 fs. To achieve a SNOM observation of such fast dynamics in the individual nanoparticles, we have to overcome serious dispersion effects arising from the optical components involved, especially from the optical fiber of the SNOM probe. We achieved that by combining the conventional dispersion compensation devices composed of prism and grating pairs with adaptive pulse shaping technique, and succeeded in delivering sub-20-fs pulses to the near-field aperture with a spatial resolution of ~100 nm.[1] At present we have obtained pulses of less than 15 fs FWHM at the near-field aperture. We are conducting position-dependence measurements for the dephasing time of localized plasmons for single gold nanorods.

References

1) H. Okamoto, *Bull. Chem. Soc. Jpn.* **86**, 397–413 (2013).
2) H. Okamoto and K. Imura, *J. Phys. Chem. Lett.* **4**, 2230–2241 (2013).
3) K. Imura, K. Ueno, H. Misawa and H. Okamoto, *J. Phys. Chem. C* **117**, 2449–2454 (2013).
4) T. Shimada, K. Imura, H. Okamoto and M. Kitajima, *Phys. Chem. Chem. Phys.* **15**, 4265–4269 (2013).
5) S. Kim, K. Imura, M. Lee, T. Narushima, H. Okamoto and D. H. Jeong, *Phys. Chem. Chem. Phys.* **15**, 4146–4153 (2013).
6) T. Narushima and H. Okamoto, *Phys. Chem. Chem. Phys.* **15**, 13805–13809 (2013).

Design and Reconstruction of Molecular Quantum States of Motion

Department of Photo-Molecular Science
Division of Photo-Molecular Science I

OHSHIMA, Yasuhiro
Professor

MIZUSE, Kenta
Assistant Professor

FUJIWARA, Masanori
IMS Research Assistant Professor

HAYASHI, Masato	Post-Doctoral Fellow
MIYAKE, Shinichiro	Post-Doctoral Fellow
INAGAKI, Itsuko	Secretary

Molecules are vital existence. In a gas-phase ensemble at room temperature, they are, in an average, flying away by a few hundred meters, making turns almost reaching to 10^{11} times, and shaking themselves more than 10^{13} times within the duration of only one second. The ultimate goal this research group has been aiming to is to capture the lively figures of molecules moving in such a dynamic manner and to have a perfect command over the molecular motions. Here lasers with ultimate resolution in time and energy domains are employed complementally and cooperatively for this purpose.

1. Nonadiabatic Excitation of Molecular Rotation Induced by Intense Ultrashort Laser Fields

When a gaseous molecular sample is irradiated by an intense nonresonant ultrashort laser pulse, the rotation of the molecules is coherently excited to create a rotational quantum wave packet (WP). We developed a method to explore the nonadiabatic excitation in a quantum-state resolved manner and applied it to diatomic and symmetric-top molecules.[1)] It has been shown that the state distribution is a useful experimental source for verifying the excitation process.[2,3)] When a pair of excitation pulses is implemented, partial control of rotational-state distribution has been achieved.[1,4)] In a favorable case, the double-pulse excitation has enabled us to reconstruct experimentally a rotational WP thus created.[5)] The sense of rotation can also be controlled, yielding to a rotational WP exhibiting angular-momentum orientation.[6,7)]

2. Coherent Excitation of Intermolecular Vibrations by Nonresonant Intense Ultrashort Laser Fields

Nonadiabatic interaction with an intense ultrashort laser field can also coherently excite vibration of molecule. We have succeeded in creating and observing WPs pertinent to intermolecular vibrations of several molecular clusters in their vibronic ground states.

3. Construction of an Ion-Imaging Apparatus for Wave Packet Imaging

We have constructed an ion-imaging apparatus for tracking the time-dependent molecular alignment by monitoring the 2D spatial distribution of Coulomb-exploded fragment ions. In the apparatus, ion clouds are repelled perpendicularly to hit a 2D detector, of which detection plate is set parallel along the initial flight direction of the ions. This unique arrangement allows us to record ion images for non-cylindrically symmetric fragment distribution. By using this experimental setup, we have monitored spatiotemporal propagation of the molecular alignment of jet-cooled N_2.

4. High-Resolution Laser Spectroscopy of Benzene Clusters with Atoms and Small Molecules[8,9)]

As prototypical systems for elucidating the intermolecular interaction pertinent to aromatic rings, we studied clusters of benzene with small numbers of atoms and molecules (such as He and H_2), by exploring via two-color resonant two-photon ionization in the vicinity of the monomer S_1–S_0 6_0^1 band. Extensive adiabatic cooling with the rotational temperature of < 0.5 K was conducted by the high-pressure pulsed expansion. Sub-Doppler resolution yielding the line width of 250 MHz was realized in a collimated molecular beam by employing Fourier-transform-limited ultraviolet pulses for the excitation.

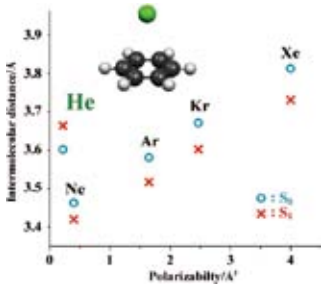

Figure 1. The effective intermolecular distances in the benzene–rare gas complexes.

The observed transition frequencies of benzene–$(He)_n$ with n = 1 and 2 were fitted to derive the molecular constants with accuracy improved by a factor of 50 than those reported previously.[10] The determined rotational constants for n = 1 set the distance of the He atom from the benzene ring, which is even larger than those of the analogous systems, *i.e.*, benzene–Ne and –Ar, as shown in Figure 1. This apparent anomaly is discussed with the recent theoretical results based on high-level quantum mechanical calculation coupled with the numerical solution of the 3D eigenvalue problem.[11] The electronic excitation induces the increase in the distance for benzene–He, as opposed to the contraction of other benzene–rare gas systems. The distance and the change for n = 2 are almost the same as those for n = 1. We also recorded the excitation spectrum of n = 1 with the mono ^{13}C-substituted benzene. The asymmetric substitution lifts the degeneracy of the S_1 6^1 state in the benzene molecule, and two vibronic bands located nearby to each other were observed.

For C_6H_6–$(H_2)_n$, two distinguished isomers, correlating to *para* and *ortho* H_2, are identified for n = 1 and 2. This finding is the manifestation of the internal rotation of the H_2 unit(s) located above (and below) the benzene molecular plane within the clusters. For the observation of the weaker binding *para* species, a gas sample of pure *para* H_2 was used. Rotationally resolved spectra allowed us to fix the cluster geometry unambiguously. Three vibronic bands involving vdW-mode excitation were observed for the *ortho* species with n = 1, yielding to probable sets of vibrational frequencies of all the three vdW modes. One of them correlates to the splitting between the m = 0 and ±1 sublevels in the j = 1 state of a freely rotating H_2 molecule, and the potential barrier for the hindered internal rotation has been evaluated from the values, as shown in Figure 2. Rotationally resolved spectrum of benzene–(*ortho* $H_2)_3$ is consistent with a (2 + 1) binding motif, where two H_2 molecules on one side of the benzene plane seem to scramble their positions and roles. All the clusters examined with rotational resolution exhibited homogeneous line broadening, which corresponds to the upper-state lifetimes in the sub-nanosecond regime, most probably due to vibrational predissociation in the S_1 6^1 manifold.

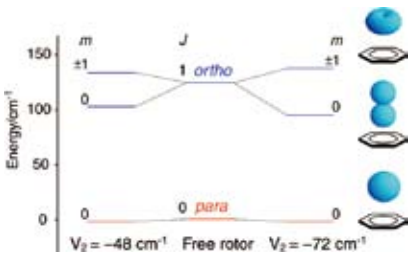

Figure 2. Schematic energy diagram for the internal rotation of H_2 inside benzene–H_2. Two probable values for the potential parameter, V_2, from the experimental results are adopted. On right, probability angular distributions of the H_2 molecular axis are schematically shown for the lowest three states.

5. Seeded Optical Parametric Amplifier for Generating Chirped Nanosecond Pulses[12]

To realize rapid adiabatic passage (RAP), which drives coherent population transfer from an initial quantum state to a target state with 100% efficiency, we constructed an optical parametric amplifier (OPA) with BiBO crystals, which was seeded by a phase-modulated cw beam in the 1,040–1,070 nm region. Two-stage pre-amplification by Yb-doped fibers were implemented for stable injection to the OPA. The frequency chirp in the OPA pulse was actively controlled, as shown in Figure 3. Down/up chirps with up to 500 MHz shift were demonstrated. The output pulse energy was ~40 mJ, which is sufficient for two-photon RAP.

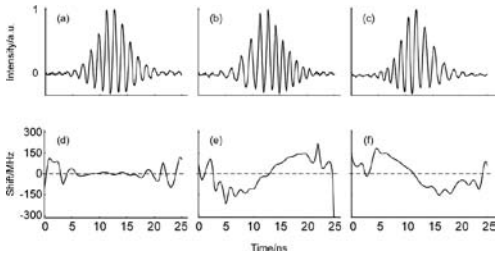

Figure 3. Observed heterodyne signals of the OPA pulses (a): without the phase modulation to the seeding beam, (b) and (c): with the phase modulation, and the time-dependent frequency shifts: (d), (e) and (f), corresponding to (a), (b) and (c), respectively.

References

1) Y. Ohshima and H. Hasegawa, *Int. Rev. Chem. Phys.* **29**, 619–663 (2010).
2) H. Hasegawa and Y. Ohshima, *Phys. Rev. A* **74**, 061401 (4 pages) (2006).
3) H. Hasegawa and Y. Ohshima, *Chem. Phys. Lett.* **454**, 148–152 (2008).
4) D. Baek, H. Hasegawa and Y. Ohshima, *J. Chem. Phys.* **134**, 224302 (10 pages) (2011).
5) H. Hasegawa and Y. Ohshima, *Phys. Rev. Lett.* **101**, 053002 (4 pages) (2008).
6) K. Kitano, H. Hasegawa and Y. Ohshima, *Phys. Rev. Lett.* **103**, 223002 (4 pages) (2009).
7) Y. Khodorkovsky, K. Kitano, H. Hasegawa, Y. Ohshima and I. Sh. Averbukh, *Phys. Rev. A* **83**, 023423 (10 pages) (2011).
8) M. Hayashi and Y. Ohshima, *Chem. Phys.* **419**, 131–137 (2013).
9) M. Hayashi and Y. Ohshima, *J. Chem. Phys. A*, in press (2013).
10) S, M. Beck, M. G. Liverman, D. L. Monts and R. E. Smalley, *J. Chem. Phys.* **70**, 232–237 (1979).
11) S. Lee, J. S. Chung, P. M. Felker, J. L. Cacheiro, B. Fernández, T. B. Pedersen and H. Koch, *J. Chem. Phys.* **119**, 12956–12964 (2003).
12) S. Miyake and Y. Ohshima, *Opt. Express* **21**, 5269–5274 (2013).

Development of High-Precision Coherent Control and Its Applications

Department of Photo-Molecular Science
Division of Photo-Molecular Science II

OHMORI, Kenji
Professor

TAKEI, Nobuyuki
Assistant Professor

GOTO, Haruka	Post-Doctoral Fellow	KOYASU, Kuniaki	Graduate Student
SOMMER, Christian	Post-Doctoral Fellow	INAGAKI, Itsuko	Secretary
NAKAGAWA, Yoshihiro	Graduate Student	YAMAGAMI, Yukiko	Secretary

Coherent control is based on manipulation of quantum phases of wave functions. It is a basic scheme of controlling a variety of quantum systems from simple atoms to nanostructures with possible applications to novel quantum technologies such as bond-selective chemistry and quantum computation. Coherent control is thus currently one of the principal subjects of various fields of science and technology such as atomic and molecular physics, solid-state physics, quantum electronics, and information science and technology. One promising strategy to carry out coherent control is to use coherent light to modulate a matter wave with its optical phase. We have so far developed a high-precision wave-packet interferometry by stabilizing the relative quantum phase of the two molecular wave packets generated by a pair of femtosecond laser pulses on the attosecond time scale. We will apply our high-precision quantum interferometry to gas, liquid, solid, and surface systems to explore and control various quantum phenomena.

1. Optically Engineered Quantum Interference of Delocalized Wavefunctions in a Bulk Solid: The Example of Solid Para-Hydrogen[1)]

Local excitations of indistinguishable particles in a solid are quantum-mechanically superposed to give delocalized wave functions. Their interference is often so short-lived that it eludes observation and manipulation. Here we have actively controlled interference of delocalized vibrational wave func-

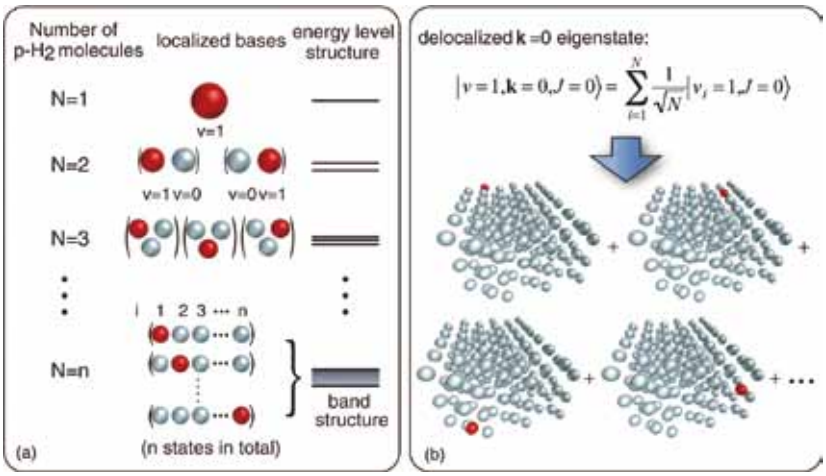

Figure 1. Formation of the delocalized vibron in solid p-H_2. (a) A band structure arises from the interaction among many indistinguishable p-H_2 molecules, one of which is vibrationally excited. The red and blue spheres stand for the vibrationally excited and ground-state p-H_2 molecules, respectively. (b) Every p-H_2 molecule within a single crystal has an equal probability to be vibrationally excited. These locally excited states $|v_i = 1\rangle$ (i = 1,...,N) are coherently superposed to give a delocalized vibron state $|v = 1, \mathbf{k} = 0\rangle$. This figure has been adopted from reference 1.

tions in solid *para*-hydrogen produced by a pair of ultrashort laser pulses. The ultrafast evolution of their interference changes from almost completely constructive (amplification by a factor of ~4) to destructive when we change the timing of those two laser pulses by only 4 fs. This active control serves as an experimental tool to investigate the spatiotemporal evolution of a wave function in a bulk solid.

2. Wavepacket Interferometry for Nuclear Densities and Flux Densities[2)]

The traditional wavepacket interferometry for nuclear densities is extended to nuclear flux densities. Accordingly, a molecule vibrating in an electronic excited state may be prepared such that at a given time, the nuclear densities correspond to a broad distribution of the molecular bond, from short to long distances, which is subdivided into a chain of lobes. We discover that neighbouring lobes, or groups of lobes, may flow towards alternating directions, implying alternating bond stretches and bond compressions. The corresponding nuclear flux densities may be controlled by appropriate parameters of the two laser pulses, which generate the underlying interferences. Similar patterns of the nuclear densities and flux densities may also be created by a single laser pulse, which may cause interferences of the overlapping tail and head of a wavepacket as they run towards or away from a turning point, respectively. The phenomena are demonstrated for the model system I_2(B).

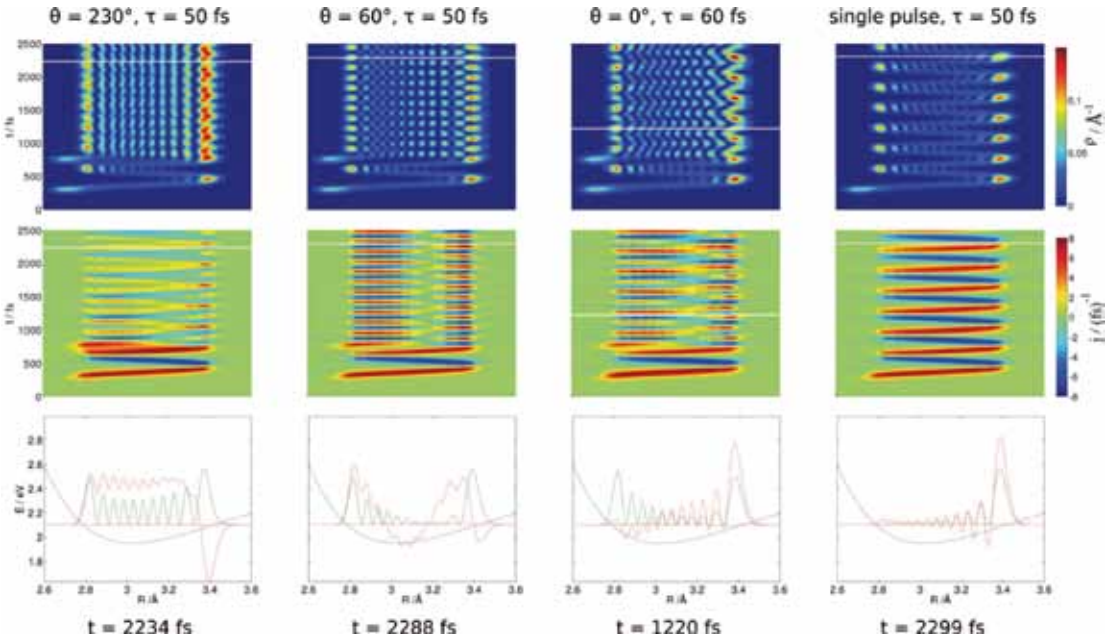

Figure 2. Wavepacket interferometry for the nuclear densities ρ(*R*, *t*) (top panels) and flux densities *j*(*R*, *t*) (middle panels) of the model I_2(B), after excitations by two sub-pulses (first three columns) or by a single pulse (last column) versus nuclear bond length *R* (abscissa) and time *t* (ordinate). The values of ρ(*R*, *t*) and *j*(*R*, *t*) are indicated by colour codes on the right-hand side. The values of the control parameters of the laser sub-pulses (the duration τ and the phase θ of the second sub-pulse) are specified above the top panels. All other parameters of the laser pulses are fixed. The bottom panels show snapshots of ρ(*R*, *t*) (green lines) and *j*(*R*, *t*) (red lines) embedded in the PES of the electronic *B*-state (blue line) at specific times, which are indicated by horizontal lines in the top panels, and specified below the bottom panels. The new phenomena are discussed in detail in the text. This figure has been adopted from reference 2.

References

1) H. Katsuki, Y. Kayanuma and K. Ohmori, *Phys. Rev. B* **88**, 014507 (2013).

2) T. Bredtmann, H. Katsuki, J. Manz, K. Ohmori and C. Stemmle, *Mol. Phys.* **111**, 1691–1696 (2013). (invited paper).

Molecular Inner-Shell Spectroscopy: Local Electronic Structure and Intermolecular Interaction

Department of Photo-Molecular Science
Division of Photo-Molecular Science III

KOSUGI, Nobuhiro
Professor

YAMANE, Hiroyuki
Assistant Professor

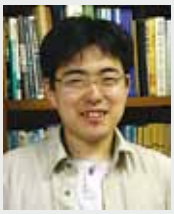

NAGASAKA, Masanari
Assistant Professor

YUZAWA, Hayato	IMS Fellow	NAKANE, Junko	Secretary
MOCHIZUKI, Kenji	Graduate Student		
WANG, Yu-Fu	Graduate Student*		

In order to reveal local electronic structures and weak intermolecular interactions in molecular systems such as organic solids, liquids, aqueous solutions, and molecular clusters, we are developing and improving several kinds of soft X-ray spectroscopic techniques, such as X-ray photoelectron spectroscopy (X-ray PES, XPS), X-ray absorption spectroscopy (XAS), resonant Auger electron spectroscopy (RAS), X-ray emission spectroscopy (XES), resonant XES (RXES), and resonant inelastic X-ray scattering (RIXS), at UVSOR in-vacuum undulator beamlines BL-3U and BL-6U with some international collaboration programs, and also an original *ab initio* quantum chemical program package GSCF, which is optimized to calculation of molecular inner-shell processes.

1. Electrochemical Reaction of Aqueous Iron Sulfate Solutions[1)]

The redox reactions of Fe ions are one of the most common electrochemical systems. Fe redox reactions have been mainly studied by voltammetric methods, but it is difficult to observe *in situ* change in valence of Fe ions in dilute electrolyte solutions. Recently, we have developed a liquid cell for soft X-ray absorption spectroscopy (XAS) in transmission mode. Furthermore, we have succeeded in development of an *in situ* XAS measurement system to study electrochemical reactions of electrolytes under realistic conditions by using a liquid cell with built-in electrodes. Change in valence of Fe ions in an aqueous iron sulfate solution at different potentials is investigated by Fe L-edge XAS.[1)]

Figure 1 shows the Fe L-edge XAS spectra of 0.5 M aqueous iron sulfate solutions at pH = 2.2 by variation of the potential at a gold electrode. Each XAS spectrum is measured at a constant potential. The XAS spectra reveal signals from Fe(II) and Fe(III) ions and show an isosbestic point, indicating only two species are involved. As seen in Figure 1(a), a nonlinear oxidation of Fe(II) to Fe(III) ions is observed when the potential is increased from 0.0 to 0.9 V. On the other hand, in Figure 1(b), the reduction of Fe(III) to Fe(II) ions shows linear dependence on the potential as decreased from 0.9 to –0.4 V.

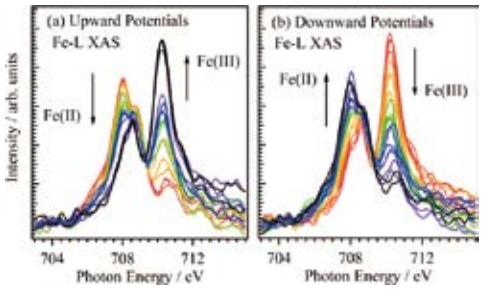

Figure 1. Fe L-edge XAS spectra of Fe ions in a 0.5 M aqueous iron sulfate at different potentials: (a) increasing from 0.00 to 0.90 V and (b) decreasing from 0.90 to –0.40 V.

Figure 2 shows the fraction of Fe(II) ions from total Fe ions as a function of potential and scanning direction, which is obtained from the XAS spectra. The fraction of Fe(II) ions decreases with increasing potential. Two processes are found in this oxidation process. The process at a high potential (0.72 V) is simple oxidation of Fe(II). The process at a low potential (0.34 V) involves the sulfate ions. The peak positions are dependent on the scanning rate because the rate of this process is dominantly influenced by the sulfate ions, which affect

electrode kinetic parameters and diffusion coefficients. On the other hand, the formation of Fe(II) with decreasing potential is a simple reduction of Fe(III) ions. We have discussed the mechanism of these Fe redox processes by correlating the XAS results with cyclic voltammetry results at different scanning rates.

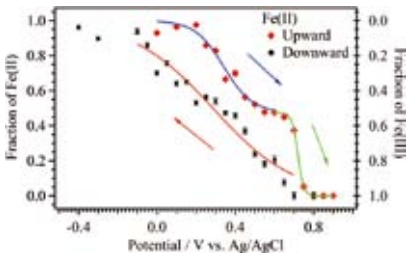

Figure 2. Fraction of Fe(II) ions as a function of potential and scanning direction versus Ag/AgCl with saturated KCl solutions.

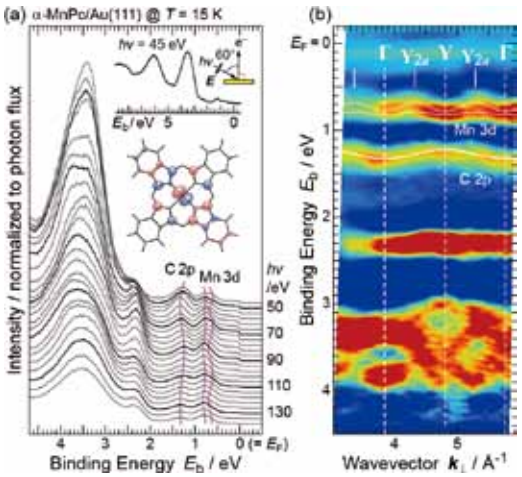

Figure 3. (a) $h\nu$-dependent normal-emission ARPES spectra ($h\nu$ step = 4 eV) of the MnPc crystalline film on Au(111) at 15 K. Inset shows the experimental geometry, wide valence-band spectrum at $h\nu$ = 45 eV, and the spatial distribution of the HOMO of MnPc. (b) Valence band map obtained from the second derivative of the ARPES spectra, with the tight-binding fitting (white curve).

2. Substituent-Induced Intermolecular Interaction in Organic Crystals Revealed by Precise Band-Dispersion Measurements[2)]

The intermolecular band dispersion, originating from the periodicity of the molecular stacking structure, is essential to investigate the charge transport mechanism related to organic electronics. Recently, we have succeeded in observation of quite small intermolecular band dispersions for crystalline films of metal phthalocyanine (MPc, M = metal) by the precise angle-resolved photoemission spectroscopy (ARPES) experiments.[2)] These observations enable us to perform systematic study of the intermolecular interaction in terms of the intermolecular distance along the π-π stacking direction ($a_\perp$) by changing terminal groups or central metals in MPc.

Figure 3(a) shows the photon energy ($h\nu$) dependence of normal-emission ARPES for the crystalline MnPc film on Au(111) at 15 K. The highest occupied molecular orbital (HOMO, Mn 3d) and HOMO-1 (C 2p) derived peaks of MnPc show a clear periodic shift. Moreover, we have found that the Mn 3d derived peak consists of two components with the different dispersion, indicating the relatively strong interaction at the Mn site. Figure 3(b) shows the valence band map for the crystalline MnPc film on Au(111), wherein the symmetric Γ and Y points are estimated from the lattice constant of 3.27 Å from the X-ray diffraction. The agreement between the periodicity of C 2p peak and the symmetric points indicates that the observed dispersion is ascribed to the intermolecular interaction. For the Mn 3d peak, the peak split and its dispersion are clearly seen in the band map. Furthermore, the periodicity of the Mn 3d dispersion is 1/2 times of that of the C 2p dispersion as labeled Y_{2a}. A possible origin of the Mn 3d dispersion is dimerization of the Mn d_π state.

From the observed band dispersions of the C-2p-derived band for crystalline films of various MPc molecules, the intermolecular transfer integral ($t_\perp$) can be evaluated with respect to the intermolecular distance ($a_\perp$) as shown in Figure 4. From the $t_\perp$-vs.-$a_\perp$ relation, we have found that (i) the $t_\perp$ value is getting large with decreasing the $a_\perp$ value due to the stronger intermolecular electronic coupling and that (ii) the $t_\perp$-vs.-$a_\perp$ relation seems to be fitted by a linear function in the present narrow $a_\perp$ range. From the least-squares fitting, the slope parameter of $t_\perp/a_\perp$ is determined to be 75±5 meV/Å for the C-2p-derived band of α-crystalline MPc films.

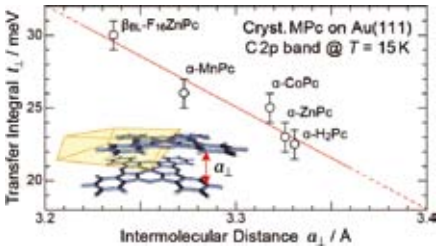

Figure 4. The $t_\perp$-versus-$a_\perp$ relation for the C 2p band in MPc crystals at 15 K obtained from the band dispersion measurement. The least-square fitting gives a slope parameter of $t_\perp/a_\perp$ = 75±5 meV/Å.

References

1) M. Nagasaka, H. Yuzawa, T. Horigome, A. P. Hitchcock and N. Kosugi, *J. Phys. Chem. C* **117**, 16343–16348 (2013).
2) H. Yamane and N. Kosugi, *Phys. Rev. Lett.* **111**, 086602 (2013).

Award

YAMANE, Hiroyuki; Young Researcher Award from National Institutes of Natural Sciences.

* carrying out graduate research on Cooperative Education Program of IMS with Tamkang University, Taiwan

Light Source Developments by Using Relativistic Electron Beams

UVSOR Facility
Division of Advanced Accelerator Research

KATOH, Masahiro
Professor

ADACHI, Masahiro
Assistant Professor

KONOMI, Taro
Assistant Professor

OHIGASHI, Takuji
Assistant Professor

TANAKA, Seiichi	Post-Doctoral Fellow	SEKITA, Sou	Graduate Student*
ARAI, Hidemi	Post-Doctoral Fellow	KAWAKAMI, Ryou	Graduate Student*
KAJIURA, Yohei	Graduate Student*		

This project involves researches and developments on synchrotron light source, free electron laser, beam physics and their related technologies, such as applications of the light sources. The most of the researches were carried out at the UVSOR facility.

1. Developments on UVSOR Accelerators

The magnetic lattice of UVSOR was modified in 2012. The new lattice gives small emittance of 15 nm-rad, which results in higher brightness of the synchrotron radiation. An in-vacuum undulator was successfully commissioned, which provides intense soft X-rays to a scanning transmission X-ray microscope (STXM). Although the storage ring was successfully commissioned in July, 2012,[1)] the machine tuning has been continued to achieve more stable operation. The beam injection efficiency has been gradually improved by the fine tuning of the injection system. Sudden beam losses frequently observed just after the commissioning have been gradually decreasing, as the vacuum conditioning via irradiation of synchrotron radiation was proceeding.

A new novel technique to inject the beam with a pulse sextupole magnet (Figure 1) was successfully demonstrated. By using this technique, the beam movement during the injection, which is inevitable with the traditional injection scheme with pulsed dipole magnets, can be avoided. As the result of the machine study just for two days, we could achieve the injection efficiency of about 20%. To introduce this scheme to the daily users operation, the efficiency should be higher than 50%. The study is going on.

Figure 1. Pulse sextupole magnet developed for UVSOR-III.

2. Improvements of STXM Beam-Line

After the successful commissioning of the STXM, the beamline BL4U (Figure 2), has been improved as an integrated system for upcoming user operation. For example, to bring out satisfactory performance of the STXM, 1) control

software of the beamline with sophisticated GUI, which makes linkage between the undulator, the monochromator and the STXM, was updated. 2) Wider energy range of incident X-rays, from 150 to 880 eV, became available by tuning the monochromator and the gap width of the undulator. 3) An experimental hutch was built at the end station of the beamline to stabilize temperature, to avoid from acoustic noise and to keep the air clean around the STXM.

On the other hand, two sample cells were designed for new applications of in-situ and polarization dependent observations. These sample cells will open new region of molecular science of the STXM.

Figure 2. BL4U Beam-line for STXM.

3. Light Source Technology Developments

We have demonstrated that coherent synchrotron radiation of various properties could be generated in an electron storage ring by using an external laser source. This research is supported by the Quantum Beam Technology Program of JST/MEXT. Under this support, a new experimental station has been constructed. The generation of coherent synchrotron radiation at the new site was successfully demonstrated. Some basic researches on coherent synchrotron radiation have been conducted as shown in Figure 3.[2] An ultrafast terahertz detector was tested.[3] Applications using coherent synchrotron radiation are under preparation and will be demonstrated in near future.

Laser Compton scattering is a method to produce monochromatic and energy-tunable gannma-ray pulses. Laser pulses are injected to the storage ring and are scattered by the relativistic electrons circulating in the ring. We developed a method to produce ultra-short gamma-ray pulses and have demonstrated a photon-induced positron annihilation lifetime spectroscopy experiment.[4]

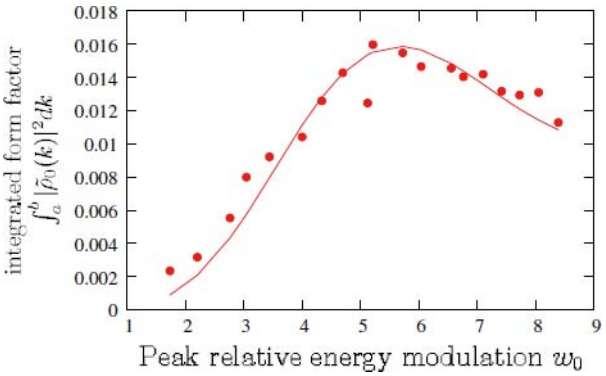

Figure 3. Observed saturation of coherent synchrotron radiation produced by the laser modulation method at UVSOR-II.

References

1) M. Adachi, H. Zen, T. Konomi, J. Yamazaki, K. Hayashi and M. Katoh, *J. Phys.: Conf. Ser.* **425**, 042013 (2013).
2) M. Hosaka, N. Yamamoto, Y. Takashima, C. Szwaj, M. Le Parquire, C. Evain, S. Bielawski, M. Adachi, T. Tanikawa, S. Kimura, M. Katoh, M. Shimada and T. Takahashi, *Phys. Rev. S. T. Accel. Beams* **16**, 020701 (2013).
3) P. Thoma, A. Scheuring, S. Wuensch, K. Il'In, A. Semenov, H-W Huebers, V. Judin, A-S. Mueller, N. Smale, M. Adachi, S. Tanaka, S. Kimura, M. Katoh, N. Yamamoto, M. Hosaka, E. Roussel, C. Szwaj, S. Bielawski and M. Siegel, *IEEE Trans. Terahertz Sci. Tech.* **3(1)**, 81–86 (2013).
4) Y. Taira, H. Toyokawa, R. Kuroda, N. Yamamoto, M. Adachi, S. Tanaka and M. Katoh, *Rev. Sci. Instrum.* **84**, 053305 (2013).

Awards

TAIRA, Yoshitaka; Young Scientist Award of the Physical Society of Japan.
TAIRA, Yoshitaka; 2012 Annual Meeting Award of the Particle Accelerator Society of Japan.
HIDA, Yohei; 2012 Annual Meeting Award of the Particle Accelerator Society of Japan.
NIWA, Takahiro; 2012 Annual Meeting Award of the Particle Accelerator Society of Japan.

* carrying out graduate research on Cooperative Education Program of IMS with Nagoya University

Synchrotron Radiation Spectroscopy on Strongly Correlated Electron Systems

UVSOR Facility
Division of Advanced Solid State Physics

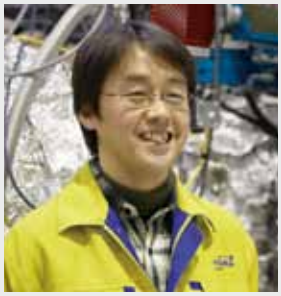

KIMURA, Shin-ichi
Associate Professor (–June, 2013)*

MATSUNAMI, Masaharu
Assistant Professor

HAJIRI, Tetsuya	Graduate Student†	KATO, Masaki	Graduate Student†
SHIMURA, Yusuke	Graduate Student†	KANEKO, Masaki	Graduate Student†
HIRATE, Satoshi	Graduate Student†	MOMIYAMA, Hakuya	Graduate Student†

Solids with strong electron–electron interaction, namely strongly correlated electron systems (SCES), have various physical properties, such as non-BCS superconducting, colossal magneto-resistance, heavy fermion and so on, which cannot be predicted by first-principle band structure calculation. Due to the physical properties, the materials are the candidates of the next generation functional materials. We investigate the mechanism of the physical properties as well as the electronic structure of SCES, especially rare-earth compounds, organic superconductors and transition-metal compounds, by infrared/THz spectroscopy and angle-resolved photoemission spectroscopy based on synchrotron radiation. Since experimental techniques using synchrotron radiation are evolved rapidly, the development of the synchrotron radiation instruments is also one of our research subjects.

1. Strongly Hybridized Electronic Structure of $YbAl_2$: An Angle-Resolved Photoemission Study[1)]

Heavy-fermion or valence fluctuation systems are characterized by the strong correlations of *f* electrons, resulting in an enhanced effective mass of quasiparticles due to the band renormalization effect. Consequently, the band structure and Fermi surface (FS) topology are modified from those predicted in band structure calculations based on local density approximation (LDA). To estimate the band renormalization effect, a direct comparison of the experimental band structure as well as the FS with the calculations is necessary. Angle-resolved photoemission spectroscopy (ARPES), which can probe both band structure and FS, is the most suitable tool for this purpose. Here we reported the electronic structure of a prototypical valence fluctuation system, $YbAl_2$, which is known as one of the prototypical valence fluctuation systems, using ARPES. In a recent hard X-ray photoemission spectroscopy study, the mean valence of Yb ions was estimated as +2.2 below 300 K. Correspondingly, an extremely high Kondo temperature (T_K) exceeding 2000 K has been suggested by the magnetic susceptibility or the inelastic neutron scattering. The mass enhancement factor is particularly small among heavy-fermion systems known so far, implying the small renormalization effect. Thus, $YbAl_2$ can be a suitable system to investigate the applicable limit of LDA calculation in relation with the fluctuating valence for the heavy-fermion systems. The observed band dispersions shown in Figure 1 are well described in terms of band structure calculations based on LDA calculation. Strong hybridization between the conduction and 4*f*

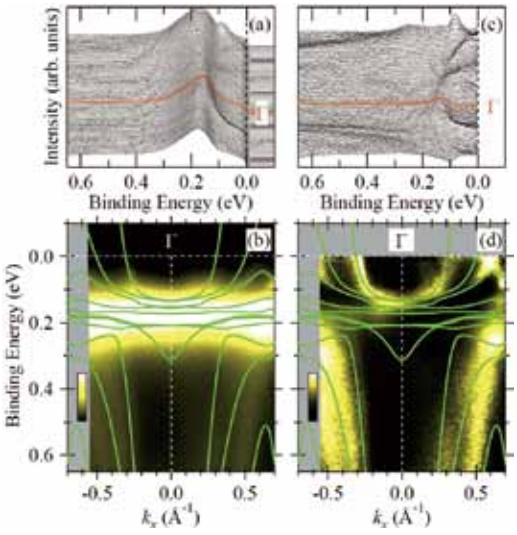

Figure 1. ARPES spectra (a) and intensity plot (b) near E_F along the Γ-K direction. (c), (d) The same data as in (a) and (b), normalized to the angleintegrated spectrum. The band dispersions obtained by the LDA calculation are overlapped in (b) and (d).

bands is identified on the basis of the periodic Anderson model. The evaluated small mass enhancement factor and the high Kondo temperature qualitatively agree with those obtained from thermodynamic measurements. Such findings suggest that the strong hybridization suppresses band renormalization and is responsible for the valence fluctuations in $YbAl_2$.

2. Optical Study of Archetypical Valence-Fluctuating Eu-Systems[2)]

Intermetallic compounds based on rare earth elements with an unstable valence, especially Ce, Eu and Yb, present many unusual properties and are therefore the subject of intense research since many years. Historically, the understanding of these compounds has been dominated by a dichotomy between the Kondo lattice/intermediate valence (KL/IV) scenario for Ce-/Yb-based systems and the valence fluctuating (VF) scenario for Eu-based systems. For Ce- or Yb-based KL/IV systems the nature of the electronic states and the low-energy excitations have been intensively investigated and are relatively well understood (with the exception of the immediate vicinity of the quantum critical point) while for Eu-based VF systems this knowledge is very limited. Then, we have investigated the optical conductivity of the prominent valence fluctuating compounds $EuIr_2Si_2$ and $EuNi_2P_2$ in the infrared energy range to get new insights into the electronic properties of valence fluctuating systems. For both compounds we observe upon cooling the formation of a renormalized Drude response, a partial suppression of the optical conductivity below 100 meV and the appearance of a mid-infrared peak at 0.15 eV for $EuIr_2Si_2$ and at 0.13 eV for $EuNi_2P_2$. Most remarkably, our results show a strong similarity with the optical spectra reported for many Ce- or Yb-based heavy fermion metals and intermediate valence systems, although the phase diagrams and the temperature dependence of the valence differ strongly between Eu- and Ce-/Yb-systems. This suggests that the hybridization between 4*f*- and conduction electrons, which is responsible for the properties of Ce- and Yb-systems, plays an important role in valence fluctuating Eu-systems.

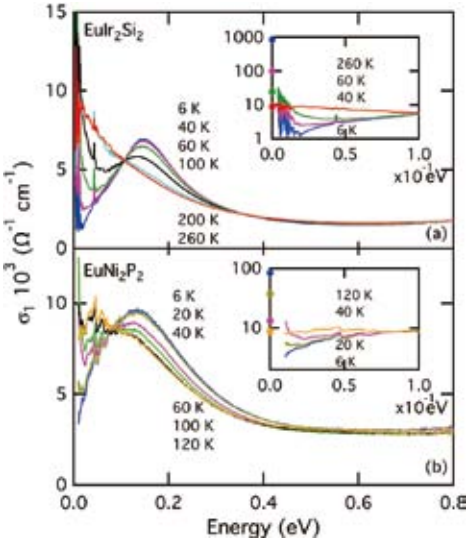

Figure 2. The real part of the optical conductivity spectra of $EuIr_2Si_2$ and $EuNi_2P_2$ at various temperatures. Insets: The low-energy optical conductivity spectra (solid lines) and the corresponding values for the dc conductivity, $\sigma_{dc} = \rho^{-1}$, (symbols) at 6, 40, 60 and 260 K for $EuIr_2Si_2$ and at 6, 20, 40 and 120 K for $EuNi_2P_2$.

3. Design of a Spin-, Symmetry-, and Momentum-Resolved Electronic Structure Analysis Instruments at UVSOR-III

UVSOR Facility equips two public undulator-beamlines for angle-resolved photoemission spectroscopy, one is BL5U in the photon energy $h\nu$ region of 20–200 eV and the other BL7U of $h\nu$ = 6–40eV. Since the monochromator of the former beamline is an old-style spherical grating type SGM-TRAIN constructed in 1990s and the throughput intensity and energy resolution are poor, the beamline was planned to be replaced to state-of-the-art monochromator and end station. Then we designed a new spin and angle-resolved photoemission spectroscopy instrument with variable photon energy and polarization. We employed a Monk-Gillieson-type variable-line-spacing plane-grating monochromator covering the photon energy of 20–200 eV. The end station shown in Figure 3 equips a VLEED spin detector. The beamline is constructed in FY2013-FY2014 and will be opened to users from FY2015.

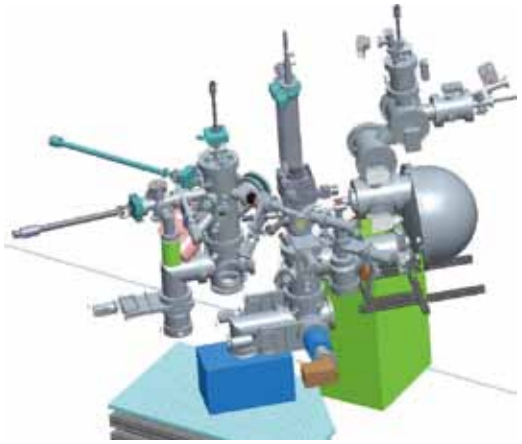

Figure 3. Schematic figure of the spin-, symmetry-, and momentum-resolved photoemission end station of BL5U, UVSOR-III.

References

1) M. Matsunami, T. Hajiri, H. Miyazaki, M. Kosaka and S. Kimura, *Phys. Rev. B* **87**, 165141 (2013).
2) V. Guritanu, S. Seiro, J. Sichelschmidt, N. Caroca-Canales, T. Iizuka, S. Kimura, C. Geibel and F. Steglich, *Phys. Rev. Lett.* **109**, 247207 (2012).

* Present Position; Professor, Graduate School of Frontier Bioscience, Osaka University
† carrying out graduate research on Cooperative Education Program of IMS with Nagoya University

Electronic Structure and Decay Dynamics in Atoms and Molecules Following Core Hole Creation

UVSOR Facility
Division of Advanced Photochemistry

SHIGEMASA, Eiji
Associate Professor

IWAYAMA, Hiroshi
Assistant Professor

The dynamics of the inner-shell photoexcitation, photoionization, and subsequent decay processes is much more complex, in comparison to outer-shell photo-processes. For instance, the inner-shell photoionization is concomitant with the excitation and ionization of valence electrons, which reveal themselves as shake-up and shake-off satellite structures in the corresponding photoelectron spectrum. The one-photon multi-electron processes, which are entirely due to the electron correlation in the system, are known to happen not only in the primary inner-shell hole creation processes, but also in their relaxation processes. Our research project is focused on elucidating the electronic structures and decay dynamics in core-excited atoms and molecules, by utilizing various spectroscopic techniques together with monochromatized synchrotron radiation in the soft x-ray region.

1. Ultrafast Dynamics in C 1s Core-Excited CF_4 Studied by Two-Dimensional Resonant Auger Spectroscopy

Excitation of a core electron to the lowest unoccupied antibonding orbital weakens the molecular bonding and populates generally a dissociative state. Morin and Nenner demonstrated that the 3d $\rightarrow \sigma^*$ excitation in HBr leads to a fast neutral dissociation which can precede the Auger relaxation; in other words, one can observe 'atomic' 3d hole decays in the Br fragment.[1)] The CF_4 molecule, tetrafluoro methane, has been a benchmark for several spectroscopic studies, due to its high symmetry, same as methane, CH_4. One of the most interesting observations deriving from the comparison between CH_4 and CF_4 is the relative intensity of below-threshold photoabsorption structures around the C 1s ionization threshold associated with transitions to empty molecular orbitals versus Rydberg states. CF_4 is a good candidate to investigate the dynamical properties of core-excited states with an electron in the antibonding lowest-unoccupied molecular orbital (LUMO) in a highly symmetric system.

Here an investigation of ultrafast dissociation following C1s-to-LUMO core excitation in CF_4, with high-resolution resonant Auger spectroscopy, is presented. The main novelty of this work is the use of two-dimensional (2D) maps to record resonant Auger spectra across the resonance as a function of photon energy with a small energy step and then to characterize ultrafast dynamics. This method allows one to follow in great detail the evolution of the resonant enhancement of spectral features corresponding to final ionic states while scanning the energy across the resonance, and to fully exploit the so-called detuning effects.

The experiment was performed on the soft X-ray beamline BL6U at UVSOR. The photon energy resolutions were set to 10000 and 4000 for total-ion yield and 2D map measurements, respectively. Kinetic energies of the emitted electrons were measured by a hemispherical electron energy analyzer (MBS-A1). The direction of the electric vector was set to be parallel to the axis of the electrostatic lens of the analyzer. The kinetic energy resolution of the analyzer was set to 60 meV. The 2D maps were obtained by taking decay spectra at regular photon energy intervals of 100 meV across the resonance.

Figure 1 shows the 2D map after subtraction of the non-resonant contributions, and with on-top two pseudo-absorption curves obtained by the CIS (Constant Ionic State) method, and namely plotting the integrated intensity of the two resonant features, the non-dispersive one related to the fragment and the dispersive one related to the $3t_2$ state, as a function of photon energy. The double feature with maxima at 297.7 and 298.4

eV is assigned to the Jahn-Teller-split transition to the LUMO (σ^* of t_2 symmetry), followed by the Rydberg series. It is seen that while the intensity of the molecular state closely mimics one of the absorption curve, the non-dispersive feature related to the fragment decreases in relative intensity across the resonance, and disappears in the photon energy region of the Rydberg states. Detailed calculations on the potential curves of the intermediate and final state would be needed to fully clarify this finding.

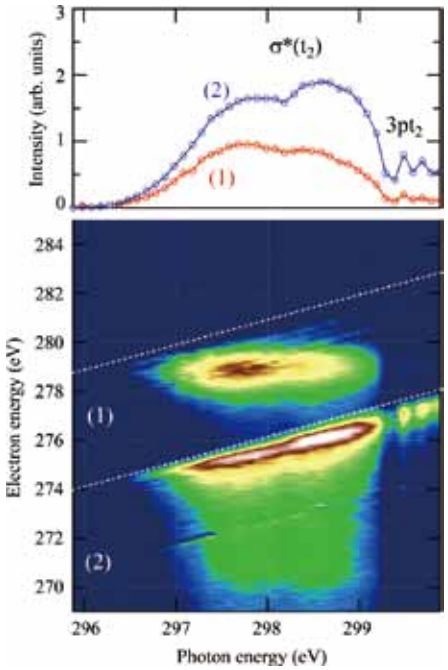

Figure 1. Top: CIS spectra of the fragment (1) and of the $3t_2$ (2) final states. Bottom: resonant Auger 2-D map showing only the resonant contributions: (1) the non-dispersive state and (2) the $3t_2$ spectral line.

2. High-Resolution Electron Spectroscopy for Ethyl Trifluoroacetate

Inner-shell photoionization of light elements is mostly relaxed via an Auger decay process, causing the emission of another electron from an outer-shell. Auger electron spectroscopy (AES) is thus an element-sensitive method with various analytical applications. Since a core hole can be regarded as being strongly localized at a particular atom, it can be expected that the Auger final dicationic state has two valence holes which are also localized near the inner-shell ionized atom. According to this simple atomic picture, the binding energies of the molecular Auger final states would also show chemical shifts. Owing to a hole–hole repulsion, the chemical shift in Auger electron spectra reflects any localization character of the two valence holes.

The interpretation of molecular Auger spectra is complex and the difficulties increase with increasing the number of atoms in a molecule. The Auger spectra become much more complicated in the case where a molecule is composed of several atoms of the same element. While well-defined photoelectron peaks reflecting the chemical shifts can be observed in photoelectron spectra, direct observations of the corresponding chemical shifts in molecular Auger spectra are practically impossible without using a coincidence technique. In order to stabilize the interpretation on the site-specific Auger spectra obtained by such coincidence experiments, however, high-resolution Auger electron spectra as well as theoretical calculations are indispensable. We have carried out high-resolution electron spectroscopic measurements on ethyl trifluoroacetate ($C_4H_5F_3O_2$).

The experiment was performed on the soft X-ray beamline BL6U at UVSOR. The radiation from an undulator was monochromatized by a variable included angle varied line-spacing plane grazing monochromator. The monochromatized radiation was introduced into a cell with sample gases. Kinetic energies of the emitted electrons were measured by a hemispherical electron energy analyzer (MBS-A1) placed at a right angle with respect to the photon beam direction. The direction of the electric vector was set to be parallel to the axis of the electrostatic lens of the analyzer. The energy resolution of the analyzer was set to 20 meV.

The oxygen and fluorine Auger electron spectra are displayed in Figure 2 (a) and (b), respectively. It is seen that the populations of the Auger final states strongly depend on which core electron is ionized. No fine structure is found in every Auger electron spectrum, in spite of the high-resolution. The Auger spectra have been simulated using a statistical approach. It is found that all Auger decays populate mainly localized dicationic states, with the two holes located either on the same fluorine atom or on adjacent fluorine atoms. While the decay of the F 1s hole populates exclusively the former states, the latter class of states is also populated by the decay of the C and O 1s holes.

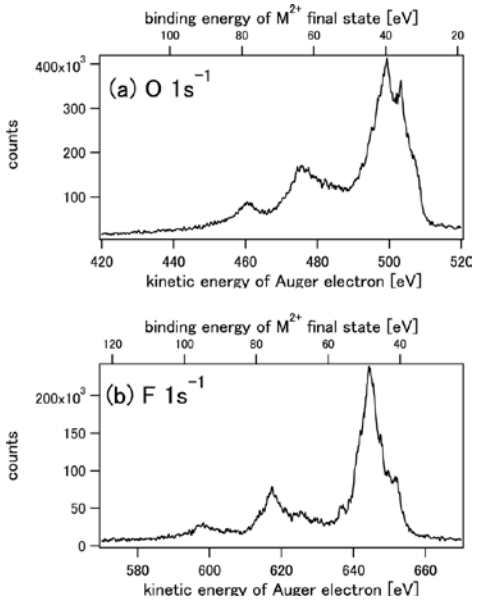

Figure 2. (a) Oxygen and (b) fluorine Auger electron spectra of $C_4H_5F_3O_2$.

References

1) P. Morin and I. Nenner, *Phys. Rev. Lett.* **56**, 1913–1916 (1986).
2) M. N. Piancastelli *et al.*, *J. Chem. Phys.* **138**, 234305 (2013).
3) H. Iwayama *et al.*, *J. Chem. Phys.* **138**, 024306 (2013).

Micro Solid-State Photonics

Laser Research Center for Molecular Science
Division of Advanced Laser Development

TAIRA, Takunori
Associate Professor

ISHIZUKI, Hideki
Assistant Professor

TSUNEKANE, Masaki	Post-Doctoral Fellow	BHANDARI, Rakesh	Post-Doctoral Fellow
SATO, Yoichi	Post-Doctoral Fellow	ARZAKANTSYAN, Mikayel	Post-Doctoral Fellow
KAUSAS, Arvydas	Post-Doctoral Fellow	KONG, Weipeng	Graduate Student
		ONO, Yoko	Secretary
		INAGAKI, Yayoi	Secretary

The artistic optical devices should be compact, reliable, efficient and high power light sources. With the approaches of domain structures and boundaries engineering, it is possible to bring the new interaction in their coherent radiation. The high-brightness nature of Yb or Nd doped single crystal or ceramic microchip lasers can realize efficient nonlinear wavelength conversion. In addition, designed nonlinear polarization under coherent length level allows us new function, such as the quasi phase matching (QPM). The development of "***Micro Solid-State Photonics***," which is based on the micro domain structure and boundary controlled materials, opens new horizon in the laser science.

1. High Peak Power, Passively Q-Switched Yb:YAG/Cr:YAG Micro-Lasers

High peak power (>MW), passively Q-switched Yb:YAG/Cr:YAG micro-laser end-pumped by fiber-coupled 120 W QCW LDs (Repetition rate < 100 Hz) was developed. The convex output coupler with a curvature of 2 m successfully enlarged the fundamental mode size in the micro-laser cavity, and the output pulse energy increased to 3.6 mJ at a Cr:YAG initial transmission of 89% without optical damage. The TEM_{00} transverse mode and the single-frequency oscillation were confirmed. The pulse duration was 1.3 ns, and then the peak power was estimated as 2.8 MW. To our knowledge, these are the highest pulse energy and peak power ever reported in Yb:YAG/Cr:YAG micro-lasers.

2. Palm-Top Size Megawatt Peak Power UV (266 nm) Microlaser

We have developed of a very compact, highly efficient, megawatt peak power, sub-nanosecond pulse width, 266 nm ultraviolet (UV) microlaser.

It contains a specially designed passively Q-switched Nd:YAG/Cr^{4+}:YAG microchip laser whose high output peak power of 13 MW enables efficient wavelength conversion without using any optics before the nonlinear crystals. The sub-nanosecond pulse width region, which delivers high peak power of several MW even for a moderate pulse energy of a few mJ, is very useful for efficient wavelength conversion.

We achieved 73% second harmonic generation efficiency using a LiB_3O_5 (Lithium Triborate, LBO) crystal and 45% fourth harmonic generation efficiency using a β-BaB_2O_4 (β-barium borate, BBO) crystal. As a result, we obtained 650 μJ, 4.3 MW peak power, 150 ps, 100 Hz pulse output at 266 nm. We used an original design for the nonlinear crystal holders to reduce the size of the microlaser.

This palm-top size 266 nm UV microlaser will be useful for many applications, such as, photoionization, UV laser induced breakdown spectroscopy (LIBS), pulsed laser deposition and materials microprocessing.

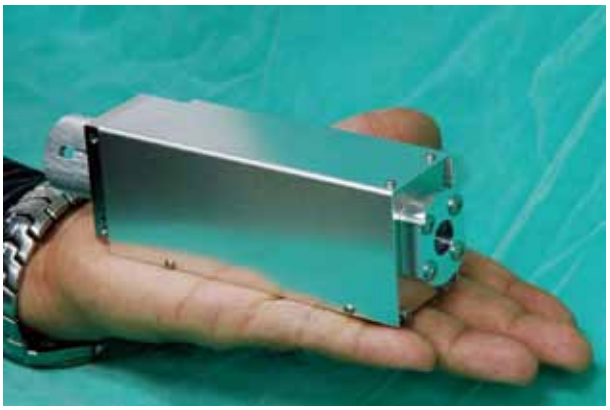

Figure 1. Palm-top size 266 nm UV microlaser.

3. Fundamental Investigations in Orientation Control Process for Anisotropic Laser Ceramics

We developed theoretical studies on the orientation control of micro-domains in anisotropic laser ceramics. The direction of the crystal axis that is parallel to easy magnetization in each micro-domain can be aligned via two steps of fabrication processes.

In the first step the alignment is performed during the slip-casting under the magnetic field, where directions of easy magnetization in primary particles are forced to align along applied magnetic field. The further orientation control can be processed by the preferential grain growth, where an adequate orientation distribution of primary articles in the casted green body is required for the nearly perfect alignment in sintered ceramics.

However, even though rare-earth trivalent ions doped into primary particles as luminous ions enhance their magnetic moment, the perfect alignment control is not always possible due to Brownian fluctuations by slurry solvent at this stage. By means of the distribution function for the crystal orientation in micro-domains under magnetic field, we confirmed the improvement in the orientation distribution contributed by preferential grain growth from detailed XRD analyses.

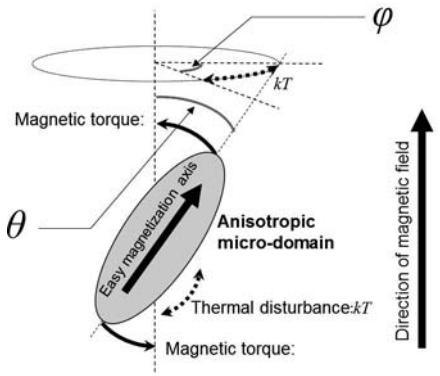

Figure 2. Conceptual diagram for the orientation control of anisotropic laser ceramics. Angle θ and φ are the angle between the control axis and the direction of easy magnetization axis and the precession angle of the micro-domain, respectively.

4. Half-Joule Output Optical-Parametric Oscillation by Using 10-mm-Thick PPMgLN Device

We presented a next generation of large-aperture periodically poled Mg-doped $LiNbO_3$ (PPMgLN) device with 10-mm thickness. Efficient optical parametric oscillation with 540 mJ output energy at 709 mJ pumping by 1.064 μm laser in 10 ns operation could be demonstrated using the 10-mm-thick PPMgLN with an inversion period of 32.2 μm at total conversion efficiency > 76%. We also confirmed that degradation effect of conversion-efficiency distribution by wedged inversion structures, which is inevitable in current poling condition of the large-aperture PPMgLN, can be ignored in high-intensity operation.

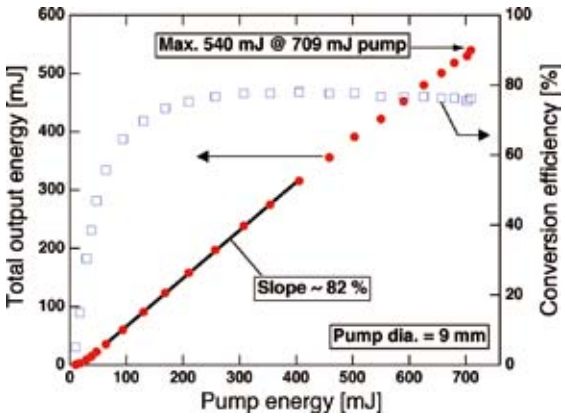

Figure 3. Characteristics of 10 nanoseconds OPO by using 10-mm-thick PPMgLN device.

References

1) M. Tsunekane and T. Taira, *IEEE J. Quantum Electron.* **49**, 454–461 (2013).
2) R. Bhandari and T. Taira, *Opt. Eng.* **52**, 076102 (6 pages) (2013).
3) Y. Sato, J. Akiyama and T. Taira, *Phys. Status Solidi C* **10**, 896 (2013), Y. Sato, J. Akiyama and T. Taira, *Opt. Mater. Express* **3**, 829 (2013).
4) H. Ishizuki and T. Taira, *Opt. Express* **20**, 20002–20010 (2012).

Ultrafast Laser Science

Laser Research Center for Molecular Science
Division of Advanced Laser Development

FUJI, Takao
Associate Professor

NOMURA, Yutaka
Assistant Professor

SHIRAI, Hideto IMS Fellow
KAWAI, Shigeko Secretary

Speed of ultrafast energy transfer from light to molecules (*i.e.* primary processes of photosynthesis, photoisomerization in visual pigments, *etc.*) is on the order of femtosecond (10^{-15} s). In our laboratory, we develop cutting edge lasers for such ultrafast molecular science, namely, femtosecond or attosecond (10^{-18} s) ultrashort pulse lasers.

For example, arbitrary waveform synthesis can be performed with simultaneous generation of femtosecond light pulses in various wavelength regions and superimposition of them with precisely controlled phases.

We would like to develop such advanced light control technology, which can push forward the research on ultrafast photochemical reactions.

1. Generation of Phase-Stable Sub-Cycle Mid-Infrared Pulses from Filamentation in Gases[1,2)]

Coherent light sources in the mid-infrared spectral region (MIR, 2.5–20 μm, 4000–500 cm^{-1}) are highly important for studies in molecular science since a number of molecular vibrations have resonance in this wavelength region. The light source can be applied to various advanced molecular spectroscopies, such as frequency comb spectroscopy for the molecular fingerprint region, pump–probe spectroscopy to trace ultrafast structural dynamics, and control of photodissociation by selective excitation of vibrational states.

Here we report the generation of sub-single-cycle pulses in the mid-infrared (MIR) region through a laser-induced filament in gases. Although the nonlinearity of gas media is much smaller than that of bulk media, the filamentation effect can be used to overcome the low efficiency. The balance between self-focusing and plasma self-defocusing in the filament makes the pulse propagate much longer than the Rayleigh range with a very high intensity. It results in a dramatic enhancement of nonlinear processes occurring in the filamentation zone.

The fundamental (ω_1) and second harmonic (ω_2) output of a 30-fs Ti:sapphire amplifier were focused into nitrogen gas and produce phase-stable broadband MIR pulses (ω_0) by using a four-wave mixing process ($\omega_1 + \omega_1 - \omega_2 \rightarrow \omega_0$) through filamentation. The spectrum spread from 400 cm^{-1} to 5500 cm^{-1}, which completely covered the MIR region. The low frequency components were detected by using an electro–optic sampling technique with a gaseous medium. The efficiency of the MIR pulse generation was very sensitive to the delay between the fundamental and second harmonic pulses. It was revealed that the delay dependence of the efficiency came from the interference between two opposite parametric processes, $\omega_1 + \omega_1 - \omega_2 \rightarrow \omega_0$ and $\omega_2 - \omega_1 - \omega_1 \rightarrow \omega_0$. The pulse duration was measured as 6.9 fs with cross-correlation frequency-resolved optical gating by using four-wave mixing in nitrogen. The carrier-envelope phase of the MIR pulse was passively stabilized. The instability was estimated as 154 mrad rms in

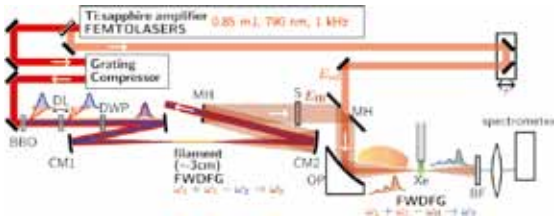

Figure 1. Schematic of the MIR pulse generation through filamentation and the chirped-pulse upconversion with FWDFG in xenon gas. BBO:β-BaB_2O_4 crystal (Type 1, θ = 29 deg, t = 100 μm), DP: delay plate (calcite crystal, t = 1.7 mm), DWP: dual wave plate (λ at 400 nm, λ/2 at 800 nm), CM1: r = 1 m concave mirror, CM2: r = 0.5 m concave mirror, MH: aluminium-coated mirror with a hole (ϕ = 7 mm), S: sample, OP: off-axis parabola (f = 50 mm), BF: blue filter.

2.5 hours. The beam profile and spectrum of the MIR field are accurately reproduced with a simple calculation based on a four-wave mixing process. Although the MIR pulse had ring-shaped beam profile, it was well-focusable. The ring-shaped pattern was originated from a dramatic confocal-parameter mismatch between the MIR field and the laser beams.

2. Single-Shot Detection of Mid-Infrared Spectra by Chirped-Pulse Upconversion with Four-Wave Difference Frequency Generation in Gases[3)]

Single-shot detection of the entire MIR supercontinuum (500–4000 cm^{-1}) with reasonable resolution has been required for the above mentioned advanced molecular spectroscopies. It is straightforward to measure the MIR spectrum with a dispersive MIR spectrometer consisting of a grating and a multichannel MIR detector. However, the bandwidth of this method has been limited to about 500 cm^{-1} due to the low sensitivity and the high cost of the multichannnel MIR detectors.

An alternative approach to detect the MIR supercontinuum with single-shot is optically converting the spectra into visible region and recording them with a visible spectrometer, which has much higher performance than the MIR spectrometers. However, the bandwidths of these upconversion methods have still been limited to about 600 cm^{-1} because of the limited phase matching bandwidth of the nonlinear solid crystals for the upconversion.

Here we report the demonstration of ultrabroadband detection of MIR spectra on a single-shot basis using chirped-pulse upconversion with gas media. By using a gas as a nonlinear medium, the detection bandwidth dramatically broadens to more than 5000 cm^{-1} due to the wide transmission range and the broadband phase matching condition of the gas medium. Although the low frequency conversion efficiency due to the low nonlinearity of the gas media is the large drawback of the method, it was possible to measure spectra over the range of MIR region, specifically 200–5500 cm^{-1}, with about 2 cm^{-1} resolution on a single-shot basis.

Experimental demonstration of the method was realized with the system shown in Figure 1. The ultrabroadband MIR continuum was generated by using FWDFG of the fundamental and the second harmonic of Ti:sapphire amplifier (790 nm, 30 fs, 0.85 mJ at 1 kHz) output through filamentation in gases, which is basically the same generation scheme as that reported in the previous section. A small portion of the fundamental pulse ($E_{ref}(t)$, 0.1 mJ, ω_1) before the compressor of the Ti:sapphire amplifier system was used as a chirped pulse. The pulse duration of the chirped pulse was estimated as 10.3 ps. The chirped pulse and the MIR pulse ($E_{IR}(t)$, ω_0) were combined with a delay time τ through a mirror with a hole. The combined beam was focused into a xenon gas at about atmospheric pressure with a parabolic mirror (f = 50 mm) and generated visible light $E_{ref}^2(t-\tau)E_{IR}^*(t)$ through an FWDFG process, $\omega_1 + \omega_1 - \omega_0 \rightarrow \omega_2$. Since gas media are centrosymmetric, it is not possible to use second-order nonlinear processes but possible to use third-order nonlinear processes for frequency conversion, such as FWDFG or four-wave sum frequency generation (FWSFG). The spot size of the chirped pulse at the focus was about 12 μm. The pulse energy of the upconverted signal was several pJ. The spectrum of the FWDFG signal at a fixed delay was measured with a conventional spectrometer with an EMCCD camera. The camera was synchronized with the repetition rate of the laser and the spectrum was measured with a single shot, namely within 1 ms.

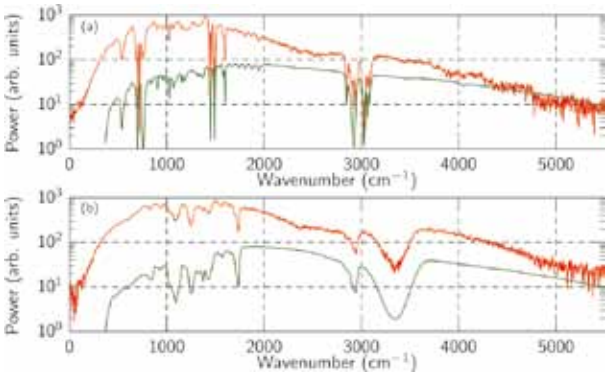

Figure 2. The spectra of the MIR pulse passed through (a) polystyrene and (b) polyvinyl alcohol films measured with the chirped pulse upconversion (red curves). The MIR absorption spectrum for each sample measured with a conventional Fourier-transform spectrometer is also shown (green curves).

We have applied the method to measure the absorption spectra of polystyrene and polyvinyl alcohol films, whose thicknesses were 38 μm and 12 μm, respectively. The MIR pulse transmitted through each film was upconverted and measured with a visible spectrometer. The path of the MIR pulse was purged with argon. The MIR spectra retrieved from the visible spectra are shown in the Figure 2. Several absorption lines of the polystyrene and polyvinyl alcohol films are clearly observed. For comparison, the MIR absorption spectrum of each sample was measured with a conventional Fourier-transform spectrometer with the resolution of 1.3 cm^{-1}. As can be seen in Figure 2, the fine structures of the MIR absorption lines are very well reproduced.

One of the most interesting applications of the chirped-pulse upconversion method is MIR spectroscopy with attenuated total reflectance (ATR) because there should be no change of temporal and spatial overlap of the MIR pulse and the chirped pulse by exchanging the sample at the chirped pulse upconversion system with the ATR.

References

1) Y. Nomura, H. Shirai, K. Ishii, N. Tsurumachi, A. A. Voronin, A. M. Zheltikov and T. Fuji, *Opt. Express* **20**, 24741–24747 (2012).
2) T. Fuji and Y. Nomura, *Appl. Sci.* **3**, 122–138 (2013).
3) Y. Nomura, Y.-T. Wang, T. Kozai, H. Shirai, A. Yabushita, C.-W. Luo, S. Nakanishi and T. Fuji, *Opt. Express* **21**, 18249–18254 (2013).

Dissociative Photoionization Studies of Fullerenes and Carbon Nanotubes and Their Application to Dye-Sensitized Solar Cells

Department of Photo-Molecular Science
Division of Photo-Molecular Science III

KATAYANAGI, Hideki
Assistant Professor

We have observed the dissociative photoionization of the fullerenes. We studied the mechanisms and kinetics of C_2 release reactions from the fullerenes on the basis of the yield curves and the scattering velocity distributions of the fragments $C_{60(70)-2n}^{z+}$ ($n \geq 1$; z = 1–3). We now intend to apply the above gas phase spectroscopy to functional materials such as carbon nanotubes (CNTs). Additionally we utilize the CNT as catalytic counter electrodes in dye-sensitized solar cells (DSSCs). This research aims at understanding the electron transfer reactions from CNTs both in gas phase and in condensed phase.

1. Mass Resolved Velocity Map Imaging of Doubly Charged Photofragments from C_{60}

We observed mass resolved velocity map images of fragments produced by the photodissociation of the fullerenes.[1,2] However we have not obtained a two-dimensional (2D) projection of three-dimensional (3D) velocity distribution of each fragment. We installed a four-element imaging lens which enables us to completely resolve the fragment signals. We thus observed the 2D velocity image of each fragment. The 2D velocity image of C_{58}^{2+} was found to be a convolution of isotropic barycentric velocity distribution of C_{58}^{2+} and anisotropic velocity of C_{60} in the parent molecular beam.

2. Gas Phase Spectroscopy of CNTs

The gas phase spectroscopy used to elucidate the dissociation dynamics of the fullerenes is now applied to the CNT. We have started to design a vacuum chamber for the gas phase spectroscopy of CNTs. Meanwhile we have examined properties and suitable vaporization conditions of CNT samples using AFM and MALDI equipment. We are also seeking for methods for controlling the length of CNT. The gas phase spectroscopy of length selected CNT will allow us to understand properties of the CNTs as functions of their length.

3. Development and Evaluation of CNT Catalytic Counter Electrodes for DSSCs

To improve photovoltaic energy conversion efficiency of the DSSC, the rate of charge transfer reaction on the counter electrode is important. We prepared the counter electrodes using commercial CNT aqueous dispersions. We found a simple method to produce the CNT counter electrodes with comparable efficiency to Pt electrodes.

References

1) H. Katayanagi and K. Mitsuke, *J. Chem. Phys. (Communication)* **133**, 081101 (4 pages) (2010).
2) H. Katayanagi and K. Mitsuke, *J. Chem. Phys.* **135**, 144307 (8 pages) (2011).

Visiting Professors

Visiting Professor
NODA, Susumu *(from Kyoto University)*

Strong Coupling of Single Atoms to Photonic Crystal Cavity Field

We have investigated photonic crystal structures which enable modification of propagation properties of an electromagnetic field and also tight confinement of the field to a tiny resonator. Accordingly the field strength inside the resonator is much enhanced and therefore the field can be strongly coupled to a quantum emitter such as a quantum dot even at a single photon level. Such a nanostructure device would be suitable for applications in optical communication and future quantum information processing in terms of its scalability. We have studied the strong coupling of the cavity field with a quantum dot and also the Purcell effect. Recently we have been interested in adopting a single cold atom as a quantum emitter, which shows much longer coherence time and therefore would be desirable for future application. Cold atoms are first loaded into a magneto-optical trap and then one of them is captured in tightly-focused optical tweezers. A movable lens-positioner can translate the position of the focal point, thereby transferring the trapped atom to the vicinity of the photonic crystal cavity. With this technique, the strong coupling of the single atom with the cavity field will be studied.

Visiting Professor
ITO, Atsushi *(from Tokai University)*

X-Ray Spectromicroscopy of Biomedical Specimens

Soft X-ray microscopy has a great advantage over other microscopies in the mapping of light elements or molecules containing such elements at high resolution. The mapping is realized by X-ray spectro-microscopy which utilizes distinctive spectral features of elements and molecules, that is, absorption edges and XANES profiles observed in the vicinity of the absorption edge. For applying this method to biomedical specimens, XANES profiles have been surveyed for a variety of biomolecules such as DNA, proteins (histone and albumin), sulfur-containing amino acids, calcium-containing biomolecules and iron-containing proteins at the C-K, N-K, O-K, S-L, Ca-L and Fe-L absorption edges. One of the most interesting and useful results obtained in this survey is that DNA and histone, a nuclear protein, exhibited significantly different spectra at the N-K edge, suggesting the possibility to image DNA and proteins in cellular nuclei separately. Spectromicroscopy at the N-K edge for a whole cell or an isolated nucleus would provide a unique method to image DNA distribution in a nucleus.

Visiting Associate Professor
TSUBOUCHI, Masaaki *(from Japan Atomic Energy Agency)*

THz Pulse Shaping by Interaction between THz Light and Photo-Induced Carrier

We are developing pulse shaping techniques in the THz frequency region to realize precise control of molecular rotation. First, we have developed the THz tomography of photo-induced carriers in a semi-conductor. Since the photo-induced carrier strongly interacts with THz light, the measurement and control of the carrier distribution and dynamics are significantly important to design THz optics. For the aim of pulse shaping, we have demonstrated an etalon with an optical shutter that can generate a THz pulse train with high efficiency. Our THz etalon consists of a Si plate as an input coupler and an ITO coated glass plate as an output coupler. After the THz pulse is transmitted from the Si plate, the Si is irradiated by a UV light to generate the plasma layer which strongly reflects the THz light. The UV light operates as an optical shutter which traps the THz pulse in the etalon cavity.

Visiting Associate Professor
HATSUI, Takaki *(from RIKEN SPring-8 Center)*

Theoretical Study on the Interaction between Matter and X-Ray Free Electron Laser

This year, we have investigated on the valence excitations of multiply ionized states for envelope measurement of X-ray free electron laser. Multiply ionized ground/excited anilines created by X-ray free electron lasers (XFELs) were analyzed by first-principles calculations. The analyses revealed that red shift of the optical absorption appear dominantly during XFEL illumination owing to the ultra-short lifetime of the core-hole states. The XFEL pulse envelope information is thus transferred from X-ray to optical frequency domain, where precise measurement is feasible. The predictions give foundation of novel pulse envelope monitor indispensable for future envelope-controlled XFEL experiments, such as seeded XFEL.